applied sciences

MDPI

Article

# Rotor Winding Short-Circuit-Fault Protection Method for VSPSGM Combining the Stator and Rotor Currents

Jian Qiao [1], Yikai Wang [1,*], Rufei He [2], Wenhui Wang [2], Xianggen Yin [1], Yumin Peng [2] and Hao Zhang [2]

1 State Key Laboratory of Advanced Electromagnetic Engineering and Technology, Huazhong University of Science and Technology, Wuhan 430074, China
2 CSG PGC Power Storage Research Institute, Guangzhou 510950, China
* Correspondence: d201880427@hust.edu.cn; Tel.: +86-151-2722-7626

**Abstract:** Rotor winding short circuit faults are common faults for variable-speed pumped-storage generator-motors (VSPSGM). At present, the exciting rotor fault protection of VSPSGM is simple and has low sensitivity. It can only act when the instantaneous value of the rotor phase current reaches three times the rated current. Therefore, it is difficult to cover some rotor winding short-circuit faults with weak fault characteristics. It is urgent to study a novel rotor winding short-circuit-fault protection method for VSPSGM. In this paper, a protection method that combines the stator and rotor currents with different frequencies is proposed. The characteristics of the stator and rotor currents before and after the fault is analyzed by using Clark transformation. On this basis, a specific protection criterion is constructed based on the discrete integral operation, which is easy to implement and not affected by the change of rotor speed. Then, the calculation method of the protection setting is proposed, considering the effect of unbalanced voltage and sensor measurement error. Simulation results show that the proposed method can reliably realize the protection of rotor winding faults. It has faster protection action speed than other methods in the same field. The protection coverage rate is over 90%.

**Keywords:** variable-speed generator-motor; rotor winding short-circuit fault; Clark transformation; protection method combined the stator and rotor currents



**Citation:** Qiao, J.; Wang, Y.; He, R.; Wang, W.; Yin, X.; Peng, Y.; Zhang, H. Rotor Winding Short-Circuit-Fault Protection Method for VSPSGM Combining the Stator and Rotor Currents. *Appl. Sci.* **2022**, *12*, 9051. https://doi.org/10.3390/app12189051

Academic Editor: Andreas Sumper

Received: 2 August 2022
Accepted: 6 September 2022
Published: 8 September 2022



## 1. Introduction

A wide range of flexible power regulations under both pumping mode and generation mode can be achieved by a variable-speed pumped-storage generator-motor (VSPSGM) [1], which is more efficient than the traditional constant-speed pumped-storage generator-motor [2]. It is a key component in building a future power system with newer energy [3]. In the 'pumped storage medium and long-term development plan 2021–2035' issued by the State Energy Administration of China, it is pointed out that 'it is necessary to explore and innovate the development mode of pumped storage and master variable speed pumped storage technology'.

At present, there are few studies on the relay protection of VSPSGM. The rotor winding of VSPSGM adopts an AC excitation structure [4]; the excitation voltage is high. In the process of high-speed rotation, the rotor winding is prone to insulation degradation, and internal short-circuit faults are easy to be generated [5]. The short-circuit faults will cause serious problems, such as partial overheating of the windings [6], abnormal vibration of the generator-motor [7], and even rotor damage [8]. Due to the large capacity of VSPSGM, the cost of the rotor equipment is very high. Thus, targeted protection schemes should be provided to avoid the economic loss caused by rotor damage.

The stator and rotor windings of VSPSGM are both multibranch structures, but the rotor winding cannot be configured with transverse differential protection and longitudinal differential protection, which are used for the stator winding. The main reason is that the internal space of the rotor is compact, and the condition of installing the current transformer at the neutral point side is not available [9]. Thus, the short-circuit fault of the rotor winding is in the 'weak protection' state. The fault is addressed by the instantaneous over-current protection of the power electronic excitation device. It can only act when the instantaneous value of the rotor phase current reaches three times the rated current, which has low sensitivity and has difficulty meeting the safety requirements. Since the working principle of the VSPSGM is similar to that of the doubly fed induction generator (DFIG), the related research on DFIG has certain reference values. In [10], a differential protection method considering the rotor current frequency is proposed for the DFIG with a flux-oriented vector control strategy. This method relies on the accurate measurement of the motor speed, which may not be suitable for the units using a voltage-oriented vector control strategy. In [11], a rotor winding interturn short-circuit-fault diagnosis method based on the change in flux observation difference before and after the fault is proposed, and the faults can be detected rapidly. In [12], the armature reaction mechanism of the air gap magnetic field in the DFIG rotor winding short circuit is analyzed. In [13], the characteristic frequencies of the stator side current are summarized for the DFIG rotor winding short-circuit fault. The above studies focus on the rotor fault diagnosis of DFIG. However, the capacity of the VSPSGM is much larger than that of the DFIG. The short-circuit current of VSPSGM is huge and the fault is more serious. Therefore, a protection method with a clear criterion is needed more for the VSPSGM. In [14], the internal fault simulation calculation model of the VSPSGM is established based on the multiloop theory. In [15], the low-frequency component of the stator branch current is used to judge whether a rotor winding short-circuit fault occurs. In [16], a specific protection criterion is proposed for the VSPSGM based on the harmonic characteristics of the circulating current between stator branches. This protection method has high reliability, but poor rapidity. The existing studies only use the electrical quantity of the stator side or the rotor side for fault identification. However, the combined protection of the stator and rotor side is a new solution. It can be combined with the stator branch circulation method to form a dual0configuration scheme of rotor main protection.

In this paper, a rotor winding short-circuit-fault protection method for VSPSGM, combining the stator and rotor currents with different frequencies, is proposed. The characteristic difference of stator and rotor current in normal operation state and rotor winding short-circuit-fault state is analyzed using Clark transformation. Then, the protection criterion of the proposed protection is constructed based on the discrete integral operation. The influence of unfavorable factors such as unbalanced voltage and measurement error on the protection is analyzed, and the determination method of the protection setting value is proposed. Finally, simulation results show that the proposed method is effective for interturn and interphase short circuit faults of rotor winding. The protection criterion is easy to implement and not affected by the change in rotor speed. It has faster protection action speed than other methods in the same field.

## 2. Characteristics Analysis of Stator and Rotor Current

The schematic diagram of VSPSGM connected to the power grid is shown in Figure 1. The stator outlet is connected to the power grid after being boosted by the main transformer, and the rotor excitation current is provided by the converter after the excitation transformer is reduced. The research object of this paper is the short-circuit-fault protection method of the rotor winding part in the figure.

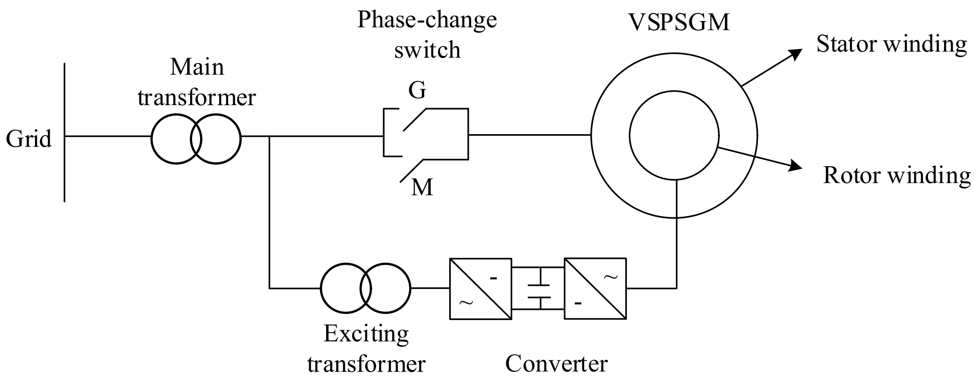


**Figure 1.** Schematic diagram of VSPSGM connected to the power grid.

*2.1. Normal Operation*

Without considering the internal structural asymmetry of the generator-motor, the stator three-phase voltages are symmetrical. The stator three-phase currents also are symmetrical and only contain the fundamental-frequency positive-sequence component. It can be recorded as:

$$\begin{aligned} i_{\mathrm{a.s}}(t) &= I_{\mathrm{s}}\cos(\omega_{\mathrm{s}}t+\varphi_{\mathrm{as}}) \\ i_{\mathrm{b.s}}(t) &= I_{\mathrm{s}}\cos\left(\omega_{\mathrm{s}}t-\tfrac{2\pi}{3}+\varphi_{\mathrm{as}}\right) \\ i_{\mathrm{c.s}}(t) &= I_{\mathrm{s}}\cos\left(\omega_{\mathrm{s}}t+\tfrac{2\pi}{3}+\varphi_{\mathrm{as}}\right) \end{aligned} \tag{1}$$

where $I_{\mathrm{s}}$ is the amplitude of the stator phase current, $\omega_{\mathrm{s}}$ is the stator angular frequency, and $\varphi_{\mathrm{as}}$ is the stator A-phase current angle.

Clark transformation is a commonly used coordinate-transformation method in the electrical analysis, which can convert the three-phase abc coordinate system to the two-phase stationary dq coordinate system. The transformation matrix is [17]:

$$\begin{bmatrix} i_{\mathrm{d.s}}(t) \\ i_{\mathrm{q.s}}(t) \end{bmatrix} = \frac{2}{3}\begin{bmatrix} 1 & -\frac{1}{2} & -\frac{1}{2} \\ 0 & \frac{\sqrt{3}}{2} & -\frac{\sqrt{3}}{2} \end{bmatrix}\begin{bmatrix} i_{\mathrm{a.s}}(t) \\ i_{\mathrm{b.s}}(t) \\ i_{\mathrm{c.s}}(t) \end{bmatrix} \tag{2}$$

Substituting Equation (1) into Equation (2), the stator-side currents $i_{\mathrm{d.s}}$ and $i_{\mathrm{q.s}}$ of the variable-speed generator-motor in the dq coordinate system can be obtained as follows:

$$\begin{aligned} i_{\mathrm{d.s}}(t) &= I_{\mathrm{s}}\cos(\omega_{\mathrm{s}}t+\varphi_{\mathrm{as}}) \\ i_{\mathrm{q.s}}(t) &= I_{\mathrm{s}}\sin(\omega_{\mathrm{s}}t+\varphi_{\mathrm{as}}) \end{aligned} \tag{3}$$

From Equation (3), the amplitudes of $i_{\mathrm{d.s}}(t)$ and $i_{\mathrm{q.s}}(t)$ are equal, and the phase difference is 90 degrees, so the following can be obtained:

$$f(i_{\mathrm{d.s}}, i_{\mathrm{q.s}}) = i_{\mathrm{d.s}}^2(t) + i_{\mathrm{q.s}}^2(t) = I_{\mathrm{s}}^2 \tag{4}$$

It can be inferred that when the generator-motor is in normal operation, the corresponding dq current instantaneous value can be obtained by performing the Clark transformation on the instantaneous value of the stator three-phase current at any time. The $f(i_{\mathrm{d.s}}, i_{\mathrm{q.s}})$ obtained by Equation (4) is always equal to the square of the amplitude of the stator-side phase current.

Similarly, the three-phase currents on the rotor side of the VSPSGM under normal operation only contains a positive sequence component, which can be denoted as:

$$\begin{aligned} i_{\mathrm{a.r}}(t) &= I_{\mathrm{r}}\cos(\omega_{\mathrm{r}}t+\varphi_{\mathrm{ar}}) \\ i_{\mathrm{b.r}}(t) &= I_{\mathrm{r}}\cos\left(\omega_{\mathrm{r}}t-\tfrac{2\pi}{3}+\varphi_{\mathrm{ar}}\right) \\ i_{\mathrm{c.r}}(t) &= I_{\mathrm{r}}\cos\left(\omega_{\mathrm{r}}t+\tfrac{2\pi}{3}+\varphi_{\mathrm{ar}}\right) \end{aligned} \tag{5}$$

where $I_r$ is the amplitude of the rotor phase current, $\omega_r$ is the rotor angular frequency, $\omega_r = s\omega_s$, $s$ is the slip ratio, the slip ratio range of the VSPSGM is usually between $\pm 0.1$, and $\varphi_{ar}$ is the rotor A-phase current angle.

After the Clark transformation, the rotor-side currents $i_{d.r}$ and $i_{q.r}$ can be obtained. Similar to Equation (4), $f(i_{d.r}, i_{q.r})$ can be constructed. When the generator-motor is in normal operation, $f(i_{d.r}, i_{q.r})$ is equal to the square of the amplitude of the rotor-side phase current.

$$f(i_{d.r}, i_{q.r}) = i_{d.r}^2(t) + i_{q.r}^2(t) = I_r^2 \tag{6}$$

The VSPSGM is essentially an induction motor. Its operating principle is similar to the transformer. Therefore, the voltage and current at the stator and rotor sides satisfy the variable ratio relationship [18]:

$$\begin{aligned} \frac{E_s}{E_r} &= \frac{1}{s}\frac{N_s k_{ws}}{N_r k_{wr}} \\ \frac{I_s}{I_r} &= \frac{N_r k_{wr}}{N_s k_{ws}} \end{aligned} \tag{7}$$

where $E_s$ and $E_r$ are the amplitudes of the stator and rotor winding's induced potential, respectively; $N_s$ and $N_r$ are the number of series turns of each branch winding on the stator and rotor sides, respectively; $k_{ws}$ and $k_{wr}$ are the fundamental wave winding factors of stator and rotor sides, respectively. Equation (7) shows that when the slip ratio $s$ changes, the induced potential ratio of the stator- and rotor-side winding changes, but the amplitude ratio of the stator and rotor phase current remains unchanged. It should be noted that Equation (7) is only satisfied under ideal conditions. In practice, the phase voltage and current of stator and rotor can be measured. Let $h = N_r k_{wr}/N_s k_{ws}$; the calculated value of $h$ should be corrected according to the measured $I_s$ and $I_r$ at normal operation.

Simultaneous to Equation (4), Equation (6), and Equation (7), the normal operation of the VSPSGM satisfies:

$$g(t) = h^2 f(i_{d.r}, i_{q.r}) - f(i_{d.s}, i_{q.s}) = 0 \tag{8}$$

where all parameters have nothing to do with the slip ratio $s$, that is, the Equation (8) is not affected by the speed change of the VSPSGM.

### *2.2. Rotor Winding Short-Circuit Fault*

A large current flows through the short-circuit ring after the fault occurs in the VSPSGM. The short-circuit current can be denoted as $i_e = I_e \cos(\omega_r t + \varphi_e)$ [16]. According to the Fourier series decomposition, the magnetomotive force generated by the short-circuit current can be decomposed as [16]:

$$\begin{aligned} F(\theta, t) &= \frac{2 I_e N_e k_{ek}}{\pi P} \sum_k \frac{1}{k} \cos(k\theta) \cos(\omega_r t + \varphi_e) \\ &= \frac{I_e N_e k_{ek}}{\pi P} \sum_k \frac{1}{k} [\cos(k\theta + \omega_r t + \varphi_e) + \cos(k\theta \omega_r t \varphi_e)] \end{aligned} \tag{9}$$

where $N_e$ is the turn number of the short-circuit coils, $k_{ek}$ is the winding factor of the short-circuit coils, $\theta$ is the space electric angle, $P$ is the number of pole-pairs, $k$ is the harmonic order, $k = 1/P, 2/P, \ldots$

It can be seen from Equation (9) that the magnetomotive force $F$ is composed of the superposition of two rotating magnetomotive forces with the same rotational speed but opposite turning directions. Among them, the forward rotating magnetomotive force will induce the positive-sequence current component in the rotor winding, while the reverse rotating magnetomotive force will induce the negative-sequence current component; both currents are equal. Therefore, the three-phase currents are no longer symmetrical after the fault, which contains some negative-sequence current components. The rotor three-phase currents after the fault can be recorded as:

$$
\begin{aligned}
i_{\mathrm{a.r}}(t) &= I_{\mathrm{r}}\cos(\omega_{\mathrm{r}}t+\varphi_{\mathrm{ar}})+I_{\mathrm{r1}}\cos(\omega_{\mathrm{r}}t+\varphi_{\mathrm{ar1}})\ +I_{\mathrm{r1}}\cos(\omega_{\mathrm{r}}t+\varphi_{\mathrm{ar1}})\\
i_{\mathrm{b.r}}(t) &= I_{\mathrm{r}}\cos\left(\omega_{\mathrm{r}}t-\tfrac{2\pi}{3}+\varphi_{\mathrm{ar}}\right)+I_{\mathrm{r1}}\cos\left(\omega_{\mathrm{r}}t-\tfrac{2\pi}{3}+\varphi_{\mathrm{ar1}}\right)+I_{\mathrm{r1}}\cos\left(\omega_{\mathrm{r}}t+\tfrac{2\pi}{3}+\varphi_{\mathrm{ar1}}\right)\\
i_{\mathrm{c.r}}(t) &= I_{\mathrm{r}}\cos\left(\omega_{\mathrm{r}}t+\tfrac{2\pi}{3}+\varphi_{\mathrm{ar}}\right)+I_{\mathrm{r1}}\cos\left(\omega_{\mathrm{r}}t+\tfrac{2\pi}{3}+\varphi_{\mathrm{ar1}}\right)+I_{\mathrm{r1}}\cos\left(\omega_{\mathrm{r}}t-\tfrac{2\pi}{3}+\varphi_{\mathrm{ar1}}\right)
\end{aligned}
\tag{10}
$$

where $I_{\mathrm{r1}}$ is the amplitude of the positive- and negative-sequence current components induced by the positive and reverse rotating magnetomotive force. The amplitude is positively correlated with the severity of the short-circuit fault. $\varphi_{\mathrm{ar1}}$ is the phase angle of the A-phase induced current.

The current $i_{\mathrm{d.r}}$ and $i_{\mathrm{q.r}}$ in the dq coordinate system after the fault can be obtained by Clark transformation:

$$
\begin{aligned}
i_{\mathrm{d.r}}(t) &= I_{\mathrm{r}}\cos(\omega_{\mathrm{r}}t+\varphi_{\mathrm{ar}})+2I_{\mathrm{r1}}\cos(\omega_{\mathrm{r}}t+\varphi_{\mathrm{ar}})\\
i_{\mathrm{q.r}}(t) &= I_{\mathrm{r}}\sin(\omega_{\mathrm{r}}t+\varphi_{\mathrm{ar}})
\end{aligned}
\tag{11}
$$

Further, $f(i_{\mathrm{d.r}}, i_{\mathrm{q.r}})$ after the rotor winding short-circuit fault can be calculated:

$$
\begin{aligned}
& f(i_{\mathrm{d.r}}, i_{\mathrm{q.r}}) = i_{\mathrm{d.r}}^2(t)+i_{\mathrm{q.r}}^2(t)\\
& = I_{\mathrm{r}}^2+2I_{\mathrm{r}}I_{\mathrm{r1}}\cos(\varphi_{\mathrm{ar}}-\varphi_{\mathrm{ar1}})\ +2I_{\mathrm{r}}I_{\mathrm{r1}}\cos(2\omega_r t+\varphi_{\mathrm{ar}}+\varphi_{\mathrm{ar1}})\ +4I_{\mathrm{r1}}^2\cos^2(\omega_r t+\varphi_{\mathrm{ar1}})
\end{aligned}
\tag{12}
$$

For the stator side, the stator phase current after the rotor winding short circuit contains a small amount of $1 \pm 2\,s$ harmonic components [19]. The stator-side three-phase current after fault can be recorded as:

$$
\begin{aligned}
i_{\mathrm{a.s}}(t) &= I_{\mathrm{s}}\cos(\omega_{\mathrm{s}}t+\varphi_{\mathrm{as}})+I_{+}\cos(\omega_{+}t+\varphi_{\mathrm{a+}})+I_{-}\cos(\omega_{-}t+\varphi_{\mathrm{a-}})\\
i_{\mathrm{b.s}}(t) &= I_{\mathrm{s}}\cos\left(\omega_{\mathrm{s}}t-\tfrac{2\pi}{3}+\varphi_{\mathrm{as}}\right)+I_{+}\cos\left(\omega_{+}t-\tfrac{2\pi}{3}+\varphi_{\mathrm{a+}}\right)+I_{-}\cos\left(\omega_{-}t-\tfrac{2\pi}{3}+\varphi_{\mathrm{a-}}\right)\\
i_{\mathrm{c.s}}(t) &= I_{\mathrm{s}}\cos\left(\omega_{\mathrm{s}}t+\tfrac{2\pi}{3}+\varphi_{\mathrm{as}}\right)+I_{+}\cos\left(\omega_{+}t+\tfrac{2\pi}{3}+\varphi_{\mathrm{a+}}\right)\ +I_{-}\cos\left(\omega_{-}t+\tfrac{2\pi}{3}+\varphi_{\mathrm{a-}}\right)
\end{aligned}
\tag{13}
$$

where $I_{+}$ and $I_{-}$ are the induced-current amplitudes of the $1 \pm 2\,s$ harmonic components at the stator side, respectively; $\varphi_{\mathrm{a+}}$ and $\varphi_{\mathrm{a-}}$ are the induced-current phase angles of the $1 \pm 2\,s$ harmonic components of phase A, respectively.

The currents $i_{\mathrm{d.s}}$ and $i_{\mathrm{q.s}}$ in the dq coordinate system after fault can be obtained by Clark transformation:

$$
\begin{aligned}
i_{\mathrm{d.s}}(t) &= I_{\mathrm{s}}\cos(\omega_{\mathrm{s}}t+\varphi_{\mathrm{as}})+I_{+}\cos(\omega_{+}t+\varphi_{\mathrm{a+}})\ +I_{-}\cos(\omega_{-}t+\varphi_{\mathrm{a-}})\\
i_{\mathrm{q.s}}(t) &= I_{\mathrm{s}}\sin(\omega_{\mathrm{s}}t+\varphi_{\mathrm{as}})+I_{+}\sin(\omega_{+}t+\varphi_{\mathrm{a+}})\ +I_{-}\sin(\omega_{-}t+\varphi_{\mathrm{a-}})
\end{aligned}
\tag{14}
$$

Further, $f(i_{\mathrm{d.s}}, i_{\mathrm{q.s}})$ after the rotor winding short circuit fault can be calculated:

$$
\begin{aligned}
& f(i_{\mathrm{d.s}}, i_{\mathrm{q.s}}) = i_{\mathrm{d.s}}^2(t)+i_{\mathrm{q.s}}^2(t)\\
& = I_{\mathrm{s}}^2+I_{+}^2+I_{-}^2+2I_{\mathrm{s}}I_{+}\cos(\omega_{\mathrm{s}}t+\varphi_{\mathrm{as}}-\omega_{+}t-\varphi_{a+})\\
& +2I_{\mathrm{s}}I_{-}\cos(\omega_{\mathrm{s}}t+\varphi_{\mathrm{as}}-\omega_{-}t-\varphi_{a-})+2I_{+}I_{-}\cos(\omega_{+}t+\varphi_{a+}-\omega_{-}t-\varphi_{a-})
\end{aligned}
\tag{15}
$$

At this time, Equation (8) is no longer established, and it is transformed into:

$$
\begin{aligned}
g(t) =\ & h^2 f(i_{\mathrm{d.r}}, i_{\mathrm{q.r}})-f(i_{\mathrm{d.s}}, i_{\mathrm{q.s}})\\
& = 2h^2 I_{\mathrm{r}}I_{\mathrm{r1}}[\cos(\varphi_{\mathrm{ar}}-\varphi_{\mathrm{ar1}})+\cos(2\omega_{\mathrm{r}}t+\varphi_{\mathrm{ar}}+\varphi_{\mathrm{ar1}})]\\
& +4h^2 I_{\mathrm{r1}}^2\cos^2(\omega_{\mathrm{r}}t+\varphi_{\mathrm{ar1}})-I_{+}^2-I_{-}^2-2I_{\mathrm{s}}I_{+}\cos(\omega_{\mathrm{s}}t+\varphi_{\mathrm{as}}-\omega_{+}t-\varphi_{a+})\\
& -2I_{\mathrm{s}}I_{-}\cos(\omega_{\mathrm{s}}t+\varphi_{\mathrm{as}}-\omega_{-}t-\varphi_{a-})-2I_{+}I_{-}\cos(\omega_{+}t+\varphi_{a+}-\omega_{-}t-\varphi_{a-})\\
& \neq 0
\end{aligned}
\tag{16}
$$

In summary, $g(t)$ is always equal to 0 under normal operation for an ideal VSPSGM. After a rotor winding short-circuit fault occurs, $g(t)$ is no longer equal to 0. The corresponding protection method can be constructed according to this feature. Since the Clark transform results are not affected by the rotor speed, the protection method does not need to take special measures for the rotor speed change.

## 3. Protection Method Combining the Stator and Rotor Currents

### *3.1. Protection Criterion*

Taking the VSPSGM of Hebei Fengning Pumped Storage Power Station as an example, its capacity is 300 MW; the pole-pairs number is 7; the rated speed is 428.6 r/min; the rotor speed range is −10%~+10%; and the power factor is 0.9. Other parameters of the VSPSGM are shown in Table 1 [16]. The mathematical analytical simulation model is established based on the multiloop method [20]:

$$p\left\{\begin{bmatrix} \boldsymbol{L}_{\mathbf{ss}} & \boldsymbol{L}_{\mathbf{sr}} \\ \boldsymbol{L}_{\mathbf{rs}} & \boldsymbol{L}_{\mathbf{rr}} \end{bmatrix}\begin{bmatrix} \boldsymbol{I}_{\mathbf{s}} \\ \boldsymbol{I}_{\mathbf{r}} \end{bmatrix}\right\} + \begin{bmatrix} \boldsymbol{R}_{\mathbf{s}} & \\ & \boldsymbol{R}_{\mathbf{r}} \end{bmatrix}\begin{bmatrix} \boldsymbol{I}_{\mathbf{s}} \\ \boldsymbol{I}_{\mathbf{r}} \end{bmatrix} = \begin{bmatrix} \boldsymbol{U}_{\mathbf{s}} \\ \boldsymbol{U}_{\mathbf{r}} \end{bmatrix} \tag{17}$$

where $p$ is a differential operator; $\boldsymbol{U}_{\mathbf{s}}$ and $\boldsymbol{U}_{\mathbf{r}}$ are the branch voltage matrices of the stator and rotor, respectively; $\boldsymbol{I}_{\mathbf{s}}$ and $\boldsymbol{I}_{\mathbf{r}}$ are the branch current matrices of the stator and rotor, respectively; $\boldsymbol{R}_{\mathbf{s}}$ and $\boldsymbol{R}_{\mathbf{r}}$ are the branch resistance matrices of the stator and rotor, respectively [21]. $\boldsymbol{L}_{\mathbf{ss}}$ is the stator inductance matrix, $\boldsymbol{L}_{\mathbf{rr}}$ is the rotor inductance matrix, $\boldsymbol{L}_{\mathbf{sr}}$ and $\boldsymbol{L}_{\mathbf{rs}}$ are the mutual inductance matrices of the stator and rotor [22]. The detailed calculation process of each parameter is shown in [23]. Equation (17) is a time-varying ordinary differential equation system, which can be solved by the fourth-order Runge–Kutta algorithm [24].

**Table 1.** The basic parameters of the VSPSGM.

| Parameter | Stator | Rotor |
|---|---|---|
| Slot number (Z) | 252 | 294 |
| Winding form | Double-layer lap winding | Double-layer wave winding |
| Number of parallel branches | 4 | 2 |
| Number of coils per branch | 21 | 49 |
| The first pitch ($y_1$) | 15 | 21 |
| The second pitch ($y_2$) | 14 | 21 |
| Rated current/A | 12,317 | 6400 |

When the slip ratio $s$ is 0.1, it is assumed that a short-circuit fault occurs between the 11th coil of the first branch of Phase A and the 8th coil of the second branch of Phase A. The coil turn difference is 3 and the fault time is 35 s. Through simulation calculation, the instantaneous waveform of stator and rotor three-phase currents are obtained, as shown in Figure 2a,b, respectively. After the fault, the stator three-phase current is dominated by fundamental frequency, containing a small amount of $1 \pm 2\,s$ harmonic components, and the rotor three-phase current changes greatly. The $f(i_{\mathrm{d.s}}, i_{\mathrm{q.s}})$ and $h^2 f(i_{\mathrm{d.r}}, i_{\mathrm{q.r}})$ obtained by the Clark transformation are shown in Figure 3. The current values in the figure are both per-unit values. The reference value is the peak current of the stator phase.

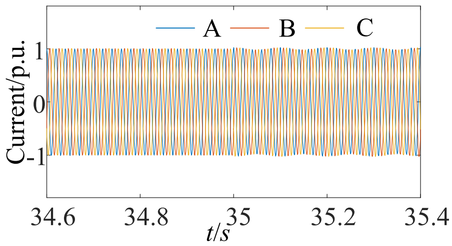


(**a**)

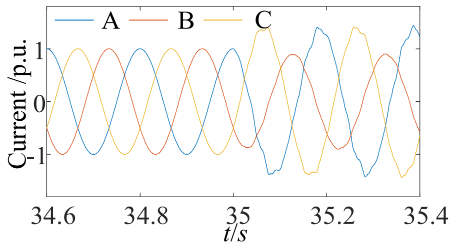


(**b**)

**Figure 2.** Three-phase currents of stator side and rotor side: (**a**) stator side; (**b**) rotor side.

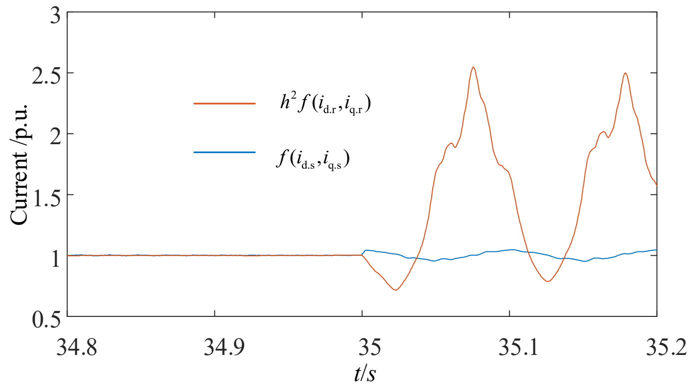


**Figure 3.** $f(i_{d.s}, i_{q.s})$ and $h^2 f(i_{d.r}, i_{q.r})$ obtained by Clark transform.

The simulation results in Figure 3 are consistent with the analysis results. After the fault occurs, $f(i_{\mathrm{d.s}}, i_{\mathrm{q.s}})$ and $h^2 f(i_{\mathrm{d.r}}, i_{\mathrm{q.r}})$ have large differences. However, the protection cannot simply use whether the difference between the two $g(t)$ is greater than a certain value as the basis for judging whether the rotor winding short-circuit fault occurs. There are two reasons: (1) $g(t)$ will change dramatically over time, and the protection setting value is difficult to set; (2) in normal operation, if there is a large measurement error in the current measurement value, $g(t)$ at that time may be too large, resulting in protection misoperation.

Aiming at the above problem, it is proposed to judge whether the fault occurs according to the size of the area around $f(i_{\mathrm{d.s}}, i_{\mathrm{q.s}})$ and $h^2 f(i_{\mathrm{d.r}}, i_{\mathrm{q.r}})$. To ensure the rapidity of the protection, the selected area calculation time window is 0.02 s (one power frequency cycle). The stator phase current of the VSPSGM is measured by the electromagnetic current transformer, and the rotor phase current is measured by Hall effect or optical current transformer. Both of them are synchronously measured and the sampling rate is consistent. One power frequency cycle is sampled $N$+1 times. In a power frequency cycle, $g$[1], $g$[2], ..., $g$[$N$+1] can be obtained by the difference between $h^2 f(i_{\mathrm{d.r}}, i_{\mathrm{q.r}})$ and $f(i_{\mathrm{d.s}}, i_{\mathrm{q.s}})$. The area calculated by the trapezoidal rule is:

$$S_{op} = \sum_{i=1}^{N} \frac{0.01}{N} (|g[i]| + |g[i+1]|) \tag{18}$$

Furthermore, the protection criterion can be expressed as:

$$S_{op} > S_{set} \tag{19}$$

where $S_{op}$ is the protection action value, $S_{set}$ is the protection setting value. To ensure the reliability of the proposed protection method, the protection setting value should avoid the maximum action value $S_{op.normal}$ of the VSPSGM under normal operation.

The steps of the proposed method are as follows:

(1) The instantaneous values of the three-phase stator and rotor currents are measured synchronously, and the dq-axis stator and rotor currents are obtained by using the Clark transform. This process is the product operation of the three-dimensional matrix, the computational burden is small, and can be realized quickly.
(2) According to Equations (12), (15) and (16), $g(t)$ is calculated by using the dq-axis stator and rotor currents, which is no longer equal to 0 after a rotor winding short-circuit fault occurs. This process is a simple algebraic operation; the computational burden is small and can be realized quickly.
(3) The protection action value $S_{op}$ is calculated according to Equation (18), and the protection outlet mode is determined according to the size of the protection action value. This process requires the protection device to have a memory storage function, which is easy to implement. The existing protection device can store the intermediate

calculation results in RAM, and can quickly exchange data with the CPU. Thus, the protection action value in Equation (18) can be obtained quickly by invoking the stored results. In addition, this process is a discrete integral operation, its algorithm is not complicated and can be realized quickly.

In summary, the computational burdens of the proposed method are small, and the conventional protection device can realize its function.

### 3.2. Calculation Method of the Protection Setting Value

The actual VSPSGM may have a slight negative-sequence component in normal operation [25], which is mainly caused by the structural asymmetry, unbalanced voltage, and sensor measurement error, so the $g(t)$ is not exactly 0. Considering that the VSPSGM will undergo strict performance index detection before leaving the factory, the negative-sequence component generated by structural asymmetry is much smaller than that generated by a large unbalanced voltage. Therefore, the influence of unbalanced voltage and sensor measurement error is mainly considered in the protection setting value calculation. The influence of unbalanced voltage is simulated by the random voltage drop of stator and rotor single-phase voltage, and the influence of the sensor measurement error factor is simulated by adding noise to each phase current obtained by simulation. The maximum action value $S_{op.normal}$ under normal operating conditions is simulated and multiplied by the reliability coefficient greater than 1 to obtain the protection setting $S_{set}$.

Taking the VSPSGM shown in Table 1 as an example, it is assumed that the single-phase voltage of the stator side drops by 1~40% randomly, and the single-phase voltage of the rotor side also drops by 1~40% randomly. A large unbalanced voltage will lead to zero-sequence voltage protection action, so the more serious voltage drop is not considered. A total of 10 dB Gaussian white noise is added to the simulated phase currents. When the slip ratio $s$ is 0.01, the maximum action value of the normal running state $S_{op.normal}$ obtained in the above scenarios is shown in Figure 4. It can be found that when the voltage drops on the stator and rotor sides, the unbalanced voltage generated will increase the protection action value $S_{op.normal}$, and the maximum value of $S_{op.normal}$ in each scenario is 0.0184. When $s$ is 0.1, the protection action value $S_{op.normal}$ in each scenario is shown in Figure 5, and the maximum value of $S_{op.normal}$ is 0.0179. It can be found that under different rotor speeds, the difference of the maximum action value $S_{op.normal}$ caused by unbalanced voltage and sensor measurement error is small, and it can be considered that the maximum $S_{op.normal}$ is almost unaffected by the rotor speed. The maximum value is selected to set the protection setting value $S_{set}$.

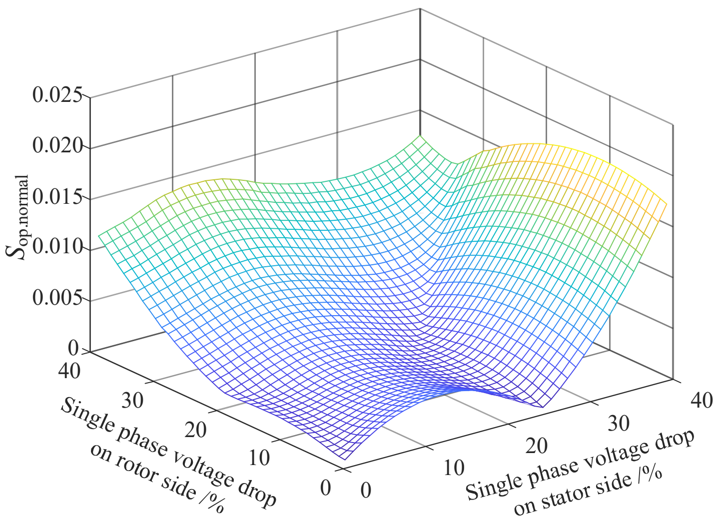


**Figure 4.** The action value $S_{op.normal}$ with different phase voltage drops when the slip ratio $s$ is 0.01.

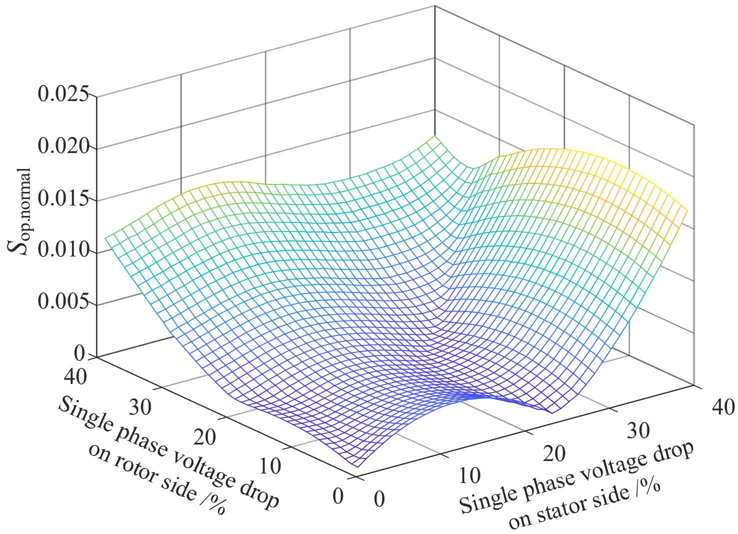


**Figure 5.** The action value $S_{op.normal}$ with different phase voltage drops when the slip ratio $s$ is 0.1.

After the above analysis, $S_{set}$ can be set to:

$$S_{\text{set}} = K_{rel} \cdot \max(S_{\text{op.normal}}) \tag{20}$$

where $K_{rel}$ is the reliability coefficient. To give the protection setting value $S_{set}$ high reliability, the value of $K_{rel}$ is set as 1.5. Then, the protection setting value $S_{set}$ is calculated to be 0.0276.

It should be noted that this method is applicable to VSPSGMs of different types, different capacities, and different winding connection forms. Of course, the protection setting values of different units are different, which need to be set according to their specific parameters, but the calculation method of protection setting values in Section 3.2 is universal. More specifically, the proposed method can be extended to the motor with three-phase AC excitation, and cannot be applied to the motor with single-phase DC excitation.

## 4. Simulation Analysis

### 4.1. Performance Analysis under Different Slip Ratios

Taking the short-circuit fault between the fourth coil of the first branch of Phase A and the ninth coil of the second branch of Phase A as an example, Equation (18) is used to calculate the protection action value, where $N$ = 48. When $s$ = 0.1, the calculation result of the protection action value $S_{op}$ is shown in Figure 6, and the protection proposed in this paper can be operated at 47.5 ms after the fault.

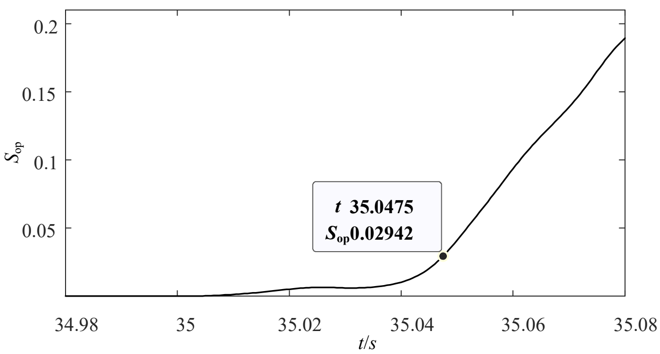


**Figure 6.** The action of the protection when the slip ratio $s$ is 0.1.

When $s$ = 0.05 and 0.01, the calculation results of the protection action value $S_{op}$ are shown in Figures 7 and 8. The protection can be operated at 91.7 ms and 365.0 ms after the fault. When the rotor speed is closer to the synchronous speed, the frequency of the rotor current is lower and closer to the DC, so that the action time of the proposed protection is gradually extended, which is inevitable. Ultimately, however, the protection method can operate correctly.

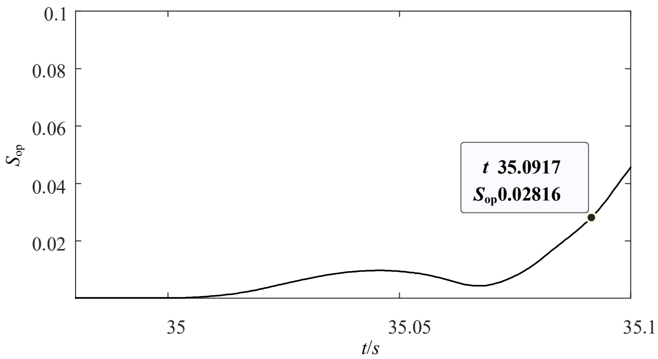


**Figure 7.** The action of the protection when the slip ratio $s$ is 0.05.

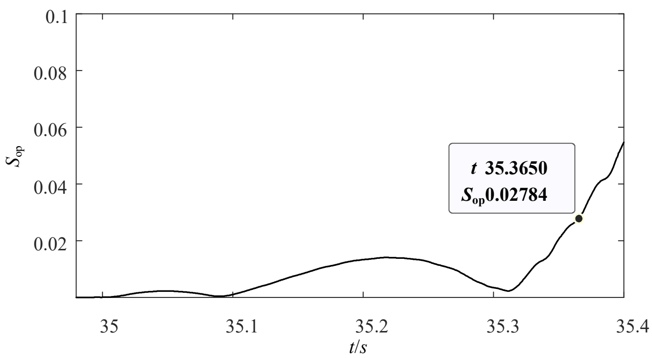


**Figure 8.** The action of the protection when the slip ratio $s$ is 0.01.

*4.2. Performance Analysis under Different Fault Types*

To verify the applicability of this method to different types of faults, it is first necessary to determine what rotor winding short-circuit faults may occur in the generator-motor. Rotor winding short-circuit faults are mainly caused by insulation damage. They can be divided into in-slot faults and end faults according to the fault position. For in-slot faults, as the name implies, the short-circuit fault occurs on two bar conductors in the same slot. The number of possible short-circuit faults is equal to the total number of slots in the rotor, denoted as $Z$. For the end faults, a specific connection form of the rotor double-layer wave windings needs to be considered, as shown in Figure 9. A single-turn coil is composed of the upper bar conductor in slot $n$ and the lower bar conductor in slot $n + y_1$. The upper connecting line of the upper bar conductor in slot $n$ is overlapped with the upper connecting line of the lower bar conductor in slot $(n + 1)$ ~$(n + y_1 - 1)$, which may lead to a total of $(y_1 - 1)$ short-circuit faults. The lower connecting line of the upper bar conductor in slot $n$ is overlapped with the lower connecting line of the lower bar conductor in the slot $(n - 1)$ ~$(n - y_2 + 1)$, which may lead to a total of $(y_2 - 1)$ short-circuit faults. There are $(y_1 + y_2 - 2)$ faults in total. Therefore, the number of short-circuit faults at the end of the whole rotor winding is $(y_1 + y_2 - 2)\ Z$.

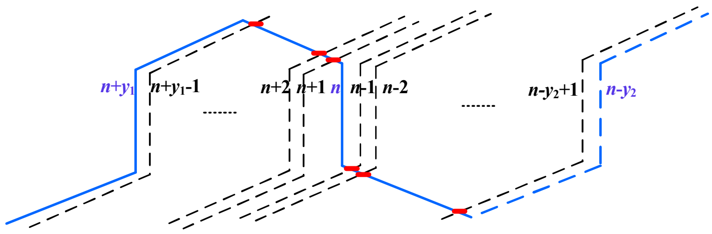


**Figure 9.** Position of the possible end short-circuit faults.

The above VSPSGM is still taken as an example. Through the statistical analysis, the number of rotor winding short-circuit faults that may occur in the unit is as shown in Table 2, and the total number of faults is 12,054.

**Table 2.** The number of possible internal short-circuit faults in rotor windings.

| | Faults in the Same Branch with Different Short Turns | Faults between Two Branches in the Same Phase | Faults between Phases | Total |
|---|---|---|---|---|
| In-slot faults | 252 | 42 | 0 | 294 |
| End faults | 1584 | 1944 | 8232 | 11,760 |
| Total | 1836 | 1986 | 8232 | 12,054 |

At present, the instantaneous over-current protection of the AC excitation system is used in engineering, as well as the rotor winding short-circuit-fault protection. The protection setting value is usually set to three times the peak value of the rated phase current of the rotor winding. When the slip ratio is 0.1, the actionable number of instantaneous over-current protections is shown in Table 3. The actionable protection number is 10,420, and the action rate is 86.44%. Among them, the action rate of interturn short-circuit faults (the faults in the same branch with different short turns + the faults between two branches in the same phase) is 63.99%, and the action rate of interphase short-circuit faults (the faults between phases) is 96.87%. The main reason for the large difference in the action rates of the two types of faults is that the fault characteristics of the interphase short circuit faults are generally more obvious and easier to protect.

**Table 3.** The actionable protection number statistical results of the existing method.

| | Faults in the Same Branch with Different Short Turns | Faults between Two Branches in the Same Phase | Faults between Phases | Total |
|---|---|---|---|---|
| In-slot faults | 205 | 35 | 0 | 240 |
| End faults | 1048 | 1158 | 7974 | 10,180 |
| Total | 1253 | 1193 | 7974 | 10,420 |

The number of actionable protections of the proposed method is 11,209, shown in Table 4, which is 789 more than that of the existing method. The sensitivity is higher, and the overall action rate is 92.98%. Among them, the action rate of interturn short-circuit fault is 85.46%, and the action rate of interphase short-circuit faults is 99.54%. Compared with the existing method, the proposed method can significantly improve the protection range of interturn short-circuit faults, and the protection action rate is increased by 21.47%.

**Table 4.** The actionable protection number statistical results of the proposed method.

| | Faults in the Same Branch with Different Short Turns | Faults between Two Branches in the Same Phase | Faults between Phases | Total |
|---|---|---|---|---|
| In-slot faults | 222 | 36 | 0 | 258 |
| End faults | 1290 | 1467 | 8194 | 10,951 |
| Total | 1512 | 1503 | 8194 | 11,209 |

*4.3. Performance Comparison with Another Method*

The reference method [16] is taken as the comparison object because it is the same as the research object of the method proposed in this paper, both of which are 300 MW variable-speed pumped-storage units.

The method in [16] is different from the method proposed in the paper in terms of implementation principle, required measurement data, and calculation burden. In terms of implementation principle, the harmonic characteristics of the circulating current between stator branches are used to judge whether a rotor winding short-circuit fault occurs [16]. In essence, the fractional harmonic magnetic field distortion inside the motor after the fault is taken as the fault characteristic. In the proposed method, the negative-sequence current of the rotor and the $1 \pm 2\,s$ component currents of the stator are mainly taken as the fault characteristics. In terms of required measurement data, the method in [16] needs to measure the three-phase branch circulation of the stator (i.e., the split-phase transverse differential current), while the proposed method needs to measure the three-phase phase current of the stator and rotor. The data sources of the two methods are different, but neither needs to install additional measuring devices. In terms of computational burden, the fractional harmonic frequencies of the method in [16] are related to the slip ratio; that is, the harmonic characteristic frequencies will change accordingly when the rotor speed changes. Therefore, it is necessary to recalculate the harmonic characteristic frequencies according to the measured rotor speed. This leads to a large computational burden on the method in [16]. However, no special treatment is required for the rotor speed in the proposed method, which makes the computational burden of the proposed method smaller.

The above differences will inevitably lead to differences in the performance of the two methods. In terms of protection action speed, the proposed method has obvious advantages over the method in [16]. The FFT algorithm is used to calculate the fractional harmonic components of the stator branch circulation in [16]. The frequency resolution of FFT is inversely proportional to the length of the time window. To overcome the influence of rotor speed on harmonic characteristic frequencies, the time window selected is longer, usually 1~5 s, and the corresponding frequency resolution is 1~0.2 Hz. However, the longer time window means that for the protection of poor speed, the action time reaches the second level. The action time of the proposed method is analyzed in Section 4.1. When the slip ratios are 0.1, 0.05, and 0.01 respectively, the protection action times of the example fault are 47.5 ms, 91.7 ms, and 365.0 ms, respectively. Its protection speed is obviously better than that of the method in [16]. Especially when the slip rate is large, the protection action time can be increased more than 10-fold.

In terms of protection coverage, the proposed method is less than the method in [16]. For the same VSPSGM, when the slip rate is 0.1, the protection action number of the method in [16] is 11,875, and the protection coverage is 98.52%. The protection action number of the proposed method is 11,209, and the protection coverage is 92.98%. Therefore, it can be said that the above two methods have their advantages and disadvantages.

Considering that the rotor short-circuit fault is a serious destructive fault, it is necessary to configure two different protection methods to realize the dual configuration scheme of the rotor's main protection. When both methods are configured, the actionable protection number of the proposed method is 11,954, as shown in Table 5. The actionable protection number is increased by 79 and 745, respectively, compared with the method in [16] and the proposed method. The total protection coverage rate can reach 99.17%. Therefore, when the two methods are configured at the same time, they can achieve complementary advantages and improve the speed and reliability of the overall protection.

**Table 5.** The actionable protection number statistical results when both methods are configured.

| | Faults in the Same Branch with Different Short Turns | Faults between Two Branches in the Same Phase | Faults between Phases | Total |
|---|---|---|---|---|
| In-slot faults | 226 | 36 | 0 | 262 |
| End faults | 1554 | 1906 | 8232 | 11,692 |
| Total | 1780 | 1942 | 8232 | 11,954 |

## 5. Conclusions

In this paper, a rotor winding short-circuit-fault protection method for VSPSGM combining the stator and rotor currents with different frequencies is proposed. The following conclusions are drawn:

(1) According to the various characteristics of stator and rotor currents before and after the rotor winding short-circuit fault, a protection method that combines the stator and rotor currents with different frequencies is proposed. This method does not need to take special treatment measures for rotor speed.

(2) The protection criterion of the proposed protection is constructed based on the discrete integral operation. Considering the influence of unbalanced voltage and sensor measurement error, the calculation method of the protection setting value is proposed to ensure the reliability of the protection method.

(3) Simulation results show that the proposed method is effective for faults with different slip ratios and different fault types. It can be combined with the stator branch circulation method to form dual protection for the internal rotor winding short-circuit fault. The protection actionable number is increased by 79 and 745, respectively, compared with the stator branch circulation method and the proposed method. The total protection coverage rate can reach 99.17%. Therefore, when the two methods are configured at the same time, they can achieve complementary advantages and improve the speed and reliability of the overall protection.

(4) The proposed method can be extended to the motor with three-phase AC excitation, and cannot be applied to the motor with single-phase DC excitation. The next work plan is to further study the protection method of dead zone faults and verify the proposed method by using the fault recorder data that may occur on the actual engineering VSPSGM in the future.

**Author Contributions:** Conceptualization, J.Q.; methodology, Y.W.; software, R.H.; validation, Y.W. and J.Q.; formal analysis, H.Z.; investigation, W.W.; resources, R.H.; data curation, J.Q.; writing—original draft preparation, Y.P.; writing—review and editing, X.Y.; visualization, Y.W.; supervision, H.Z.; project administration, W.W.; funding acquisition, R.H. All authors have read and agreed to the published version of the manuscript.

**Funding:** This research was funded by Key technology project of China Southern Power Grid Co., LTD, grant number STKJXM20210102.

**Institutional Review Board Statement:** Not applicable.

**Informed Consent Statement:** Not applicable.

**Data Availability Statement:** Not applicable.

**Conflicts of Interest:** The authors declare no conflict of interest.

## Nomenclature

| | |
|---|---|
| Acronym | |
| VSPSGM | Variable-speed pumped-storage generator-motor |
| DFIG | Doubly fed induction generator |
| RAM | Random access memory |
| CPU | Central processing unit |
| FFT | Fast Fourier transform |
| Variable/Parameter | |
| $i_{\mathrm{a.s}}$ | The stator current of phase A |
| $i_{\mathrm{b.s}}$ | The stator current of phase B |
| $i_{\mathrm{c.s}}$ | The stator current of phase C |
| $I_{\mathrm{s}}$ | The amplitude of stator phase current |
| $\omega_{\mathrm{s}}$ | The stator angular frequency |
| $\varphi_{\mathrm{as}}$ | The stator A-phase current angle |
| $i_{\mathrm{d.s}}$ | The d-axis current at stator side obtained by Clark transformation |
| $i_{\mathrm{q.s}}$ | The q-axis current at stator side obtained by Clark transformation |
| $i_{\mathrm{a.r}}$ | The rotor current of phase A |
| $i_{\mathrm{b.r}}$ | The rotor current of phase B |
| $i_{\mathrm{c.r}}$ | The rotor current of phase C |
| $I_{\mathrm{r}}$ | The amplitude of rotor phase current |
| $\omega_{\mathrm{r}}$ | The rotor angular frequency |
| $\varphi_{\mathrm{ar}}$ | The rotor A-phase current angle |
| $i_{\mathrm{d.r}}$ | The d-axis current at rotor side obtained by Clark transformation |
| $i_{\mathrm{q.r}}$ | The q-axis current at rotor side obtained by Clark transformation |
| $s$ | The slip ratio |
| $E_{\mathrm{s}}$ | The amplitudes of the stator winding induced potential |
| $E_{\mathrm{r}}$ | The amplitudes of the rotor winding induced potential |
| $N_{\mathrm{s}}$ | The number of series turns of each branch winding on the stator side |
| $N_{\mathrm{r}}$ | The number of series turns of each branch winding on the rotor side |
| $k_{\mathrm{ws}}$ | The fundamental wave winding factors of stator side |
| $k_{\mathrm{wr}}$ | The fundamental wave winding factors of rotor side |
| $I_e$ | The amplitude of short-circuit current |
| $\varphi_e$ | The angle of short-circuit current |
| $N_e$ | The turn number of the short-circuit coils |
| $k_{ek}$ | The winding factor of the short-circuit coils |
| $\theta$ | The space electric angle |
| $P$ | The number of pole-pairs |
| $k$ | The harmonic order |
| $I_{\mathrm{r1}}$ | The amplitude of the positive- and negative-sequence current components after the fault |
| $\varphi_{\mathrm{ar1}}$ | The phase angle of A-phase positive induced current after the fault |
| $I_{+}$ | The induced-current amplitudes of the 1 + 2 $s$ harmonic components |
| $I_{-}$ | The induced-current amplitudes of the $1 - 2$ $s$ harmonic components |
| $\varphi_{\mathrm{a+}}$ | The induced-current phase angles of the 1 + 2 $s$ harmonic components |
| $\varphi_{\mathrm{a-}}$ | The induced-current phase angles of the $1 - 2$ $s$ harmonic components |
| $p$ | Differential operator |
| $\boldsymbol{U}_{\mathbf{s}}$ | The stator branch voltage matrices |
| $\boldsymbol{U}_{\mathbf{r}}$ | The rotor branch voltage matrices |
| $\boldsymbol{I}_{\mathbf{s}}$ | The stator branch current matrices |
| $\boldsymbol{I}_{\mathbf{r}}$ | The rotor branch current matrices |
| $\boldsymbol{R}_{\mathbf{s}}$ | The stator branch resistance matrices |
| $\boldsymbol{R}_{\mathbf{r}}$ | The rotor branch resistance matrices |
| $\boldsymbol{L}_{\mathbf{ss}}$ | The stator inductance matrix |
| $\boldsymbol{L}_{\mathbf{rr}}$ | The rotor inductance matrix |
| $\boldsymbol{L}_{\mathbf{sr}}$ | The mutual inductance matrices of stator and rotor |
| $\boldsymbol{L}_{\mathbf{rs}}$ | The mutual inductance matrices of rotor and stator |

| | |
|---|---|
| $N$ | The sampling times in one power frequency cycle |
| $S_{op}$ | The protection action value |
| $S_{set}$ | The protection setting value |
| $S_{op.normal}$ | The maximum protection action value under normal operation. |
| $Z$ | The slot number of the VSPSGM |
| $y_1$ | The first pitch of the VSPSGM |
| $y_2$ | The second pitch of the VSPSGM |
| $K_{rel}$ | The reliability coefficient |

## References


1. Deng, Y.; Wang, P.; Morabito, A.; Feng, W.; Mahmud, A.; Chen, D.; Hendrick, P. Dynamic analysis of variable-speed pumped storage plants for mitigating effects of excess wind power generation. *Int. J. Electr. Power Energy Syst.* **2021**, *135*, 107453. [CrossRef]
2. Zhang, Z.; Cai, X. Low-carbon dispatch considering operating characteristics of variable speed pumped storage. *Pro. CSEE* **2016**, *36*, 51–60.
3. Han, X.; Ding, L.; Chen, G. Key technologies and research prospects for cascaded hydro-photovoltaic-pumped storage hybrid power generation system. *Trans. China Electrotech. Soc.* **2020**, *35*, 2711–2722.
4. Tianhui, L.; Ming, T.; Boyan, J. Modeling simulation and diagnosis analysis of inter-turn short circuits fault in generator rotor. *High Volt. Eng.* **2019**, *45*, 3932–3940.
5. Orchuk, S. Synchronous Motors: Methods for Quantifying Rotor Condition. *IEEE Ind. Appl. Mag.* **2019**, *25*, 44–54. [CrossRef]
6. Wang, L.; Li, Y.; Li, J. Diagnosis of Inter-Turn Short Circuit of Synchronous Generator Rotor Winding Based on Volterra Kernel Identification. *Energies* **2018**, *11*, 2524. [CrossRef]
7. Zhou, G.; Li, Y.; Wan, S. Analysis on rotor unbalanced electromagnetic force of generator under rotor interturn short circuit fault. *Trans. China Electrotech. Soc.* **2012**, *27*, 120–127.
8. Tang, S.; Chen, X.; Zheng, S. Fault diagnosis method of motor bearing based on attention and multi-scale convolution neural network. *Electr. Eng.* **2020**, *21*, 32–38.
9. Chen, J.; Ye, H. Research on protection of internal short circuit in rotor winding of variable speed pumped-storage generator-motor. *Electr. Power* **2021**, *54*, 121–127.
10. Mohammad, E.; Carlos, A. Novel differential protection technique for doubly fed induction machines. *IEEE Trans. Ind. Appl.* **2019**, *55*, 3697–3706.
11. Wei, S.; Ren, Z.; Fu, Y. Early stage inter-turn faults detection technique for the rotor windings of offshore wind dfigs based on the differential value of two-side linkage observation. *Pro. CSEE* **2019**, *39*, 1470–1479.
12. Abdesselam, L.; Ammar, M. Online computational tools dedicated to the detection of induction machine faults. *Int. J. Electr. Power Energy Syst.* **2013**, *44*, 752–757.
13. Stefani, A.; Yazidi, A.; Rossi, C. Double fed induction machines diagnosis based on signature analysis of rotor modulating signals. *IEEE Trans. Ind. Appl.* **2008**, *44*, 1711–1721. [CrossRef]
14. Yin, X.; Qiao, J.; Wang, Y. Optimal configuration of main protection for a variable speed pumped storage power generator based on internal fault simulation. *Power Syst Prot. Control* **2022**, *13*, 1–10.
15. Huamin, N.; Lin, G. Simulation and experimental research on internal faults of rotor winding in ac excitation generator-motor based on the multi-loop theory. *Hydropower Pumped Storage* **2021**, *7*, 34–42. Available online: https://kns.cnki.net/kcms/detail/detail.aspx?dbcode=CJFD&dbname=CJFDLAST2021&filename=DBGC202104008&uniplatform=NZKPT&v=Gq5STmDu5FoerN971O8crSHgYRMrMCI99UaXSD7sCambLWFjBzoixJVvW7CKvRsv (accessed on 1 August 2022).
16. He, R.; Qiao, J.; Peng, Y.; Yin, X.; Wang, Y.; Zhang, H.; Wang, W. A Rotor Winding Internal Short-Circuit Fault Protection Method for Variable-Speed Pumped Storage Units. *Appl. Sci.* **2022**, *12*, 7783. [CrossRef]
17. Wei, S.; Zhang, L.; Fu, Y. Early fault detection based on the Park's vector locus ovality for inter-turn faults in stator windings of the offshore wind DFIG. *Pro. CSEE* **2017**, *37*, 3001–3009.
18. Mansouri, M.; Nayeripour, M. Internal electrical protection of wind turbine with doubly fed induction generator. *Renewable Sustain. Energy Rev.* **2016**, *55*, 840–855. [CrossRef]
19. Gholam, R.; Gholam, R. Broken rotor bar and rotor eccentricity fault detection in induction motors using a combination of discrete wavelet transform and Teager–Kaiser energy operator. *IEEE Trans. Energy Convers* **2022**, *37*, 2199–2206.
20. Shiyong, X.; Baojun, G.; Zhihui, L. Multi-loop model for fractional pole-path ratio synchronous generators with stator winding internal faults. *IET Electr. Power Appl.* **2020**, *14*, 2687–2696.
21. Yuguang, S.; Wang, S. Analysis of armature inter-turn fault in the multiphase synchronous generator-rectifier system. *IET Electr. Power Appl.* **2019**, *13*, 871–880.
22. Hao, L.; Li, J. Characteristic analysis of short-circuit fault in rotor winding of nuclear power multi-phase annular brushless exciter. *Trans. China Electrotech. Soc.* **2020**, *35*, 1251–1261.
23. Huamin, N.; Lin, G.; Yuguang, S. Simulation and Experimental Research on Stator Winding Internal Faults of AC Excitation Machine Based on Multi-Loop Theory. *Pro. CSEE* **2019**, *39*, 3666–3684.

24. Lv, Z.; Wang, D.; Lin, N. Analysis and Calculation of DC Side Short-Circuit Current of High-Speed Staggered Pole Hybrid Excitation Generator. *Trans. China Electrotech. Soc.* **2020**, *35*, 1251–1261.
25. Li, W.; Qiao, J.; Wang, Y.; Liu, R.; Lv, T.; Yin, X. Fault Diagnosis Method of Stator Windings Short Circuit for Variable Speed Pumped Storage Unit Based on Park Transform. In Proceedings of the CEEPE, Chongqing, China, 22–24 April 2022; pp. 507–512. [CrossRef]